Arteriosclerosis, Thrombosis, and Vascular Biology

ORIGINAL RESEARCH

Coronary Artery Disease Risk Variant Dampens the Expression of CALCRL by Reducing HSF Binding to Shear Stress Responsive Enhancer in Endothelial Cells In Vitro

Ilakya Selvarajan (இலக்கியாசெல்வராஜன்), Miika Kiema*, Ru-Ting Huang*, Jin Li*, Jiayu Zhu, Petri Pölönen, Tiit Örd, Kadri Õunap, Mehvash Godiwala, Anna Kathryn Golebiewski, Aarthi Ravindran (ஆர்த்தி ரவீந்திரன்), Kiira Mäklin, Anu Toropainen, Lindsey K. Stolze, Maximiliano Arce, Peetra U. Magnusson, Stephen White, Casey E. Romanoski, Merja Heinäniemi, Johanna P. Laakkonen, Yun Fang, Minna Kaikkonen-Määttä

BACKGROUND: CALCRL (calcitonin receptor-like) protein is an important mediator of the endothelial fluid shear stress response, which is associated with the genetic risk of coronary artery disease. In this study, we functionally characterized the noncoding regulatory elements carrying coronary artery disease that risks single-nucleotide polymorphisms and studied their role in the regulation of *CALCRL* expression in endothelial cells.

METHODS: To functionally characterize the coronary artery disease single-nucleotide polymorphisms harbored around the gene *CALCRL*, we applied an integrative approach encompassing statistical, transcriptional (RNA-seq), and epigenetic (ATAC-seq, chromatin immunoprecipitation assay-quantitative polymerase chain reaction, and electromobility shift assay) analyses, alongside luciferase reporter assays, and targeted gene and enhancer perturbations (siRNA and clustered regularly interspaced short palindromic repeats/clustered regularly interspaced short palindromic repeat–associated 9) in human aortic endothelial cells.

RESULTS: We demonstrate that the regulatory element harboring rs880890 exhibits high enhancer activity and shows significant allelic bias. The A allele was favored over the G allele, particularly under shear stress conditions, mediated through alterations in the HSF1 (heat shock factor 1) motif and binding. CRISPR deletion of rs880890 enhancer resulted in downregulation of *CALCRL* expression, whereas HSF1 knockdown resulted in a significant decrease in rs880890-enhancer activity and *CALCRL* expression. A significant decrease in HSF1 binding to the enhancer region in endothelial cells was observed under disturbed flow compared with unidirectional flow. *CALCRL* knockdown and variant perturbation experiments indicated the role of CALCRL in mediating eNOS (endothelial NO synthase), APLN (apelin), angiopoietin, prostaglandins, and EDN1 (endothelin-1) signaling pathways leading to a decrease in cell proliferation, tube formation, and NO production.

CONCLUSIONS: Overall, our results demonstrate the existence of an endothelial-specific HSF (heat shock factor)–regulated transcriptional enhancer that mediates *CALCRL* expression. A better understanding of *CALCRL* gene regulation and the role of single-nucleotide polymorphisms in the modulation of *CALCRL* expression could provide important steps toward understanding the genetic regulation of shear stress signaling responses.

Key Words: coronary artery disease ■ coronary vessels ■ gene expression ■ genome-wide association study ■ polymorphism, single nucleotide

Correspondence to: Minna Kaikkonen-Määttä, PhD, A.I. Virtanen Institute for Molecular Sciences, University of Eastern Finland, Neulaniementie 2, 70210 Kuopio, Finland. Email minna.kaikkonen@uef.fi
*M. Kiema, R.-T. Huang, and J. Li contributed equally.
Supplemental Material is available at https://www.ahajournals.org/doi/suppl/10.1161/ATVBAHA.123.318964.
For Sources of Funding and Disclosures, see page XXX.

Arterioscler Thromb Vasc Biol is available at www.ahajournals.org/journal/atvb

Nonstandard Abbreviations and Acronyms

ADM	adrenomedullin
APLN	apelin
CAD	coronary artery disease
CALCRL	calcitonin receptor-like
CGRP	calcitonin gene-related peptide
ChIP	chromatin immunoprecipitation assay
DF	disturbed flow
EDN1	endothelin-1
eRNA	enhancer RNA
FBS	fetal bovine serum
HAEC	human aortic endothelial cell
HSF	heat shock factor
ox-LDL	oxidized low-density lipoprotein
PCR	polymerase chain reaction
PKA	protein kinase A
SNP	single-nucleotide polymorphism
UF	unidirectional flow

Highlights

- Identified a coronary artery disease risk variant (rs880890) that influences CALCRL (calcitonin receptor-like) expression through differential enhancer activity, showing a preference for the A allele.
- Demonstrated an important role of HSF1 (heat shock factor 1) in regulating CALCRL expression, where its knockdown or the deletion of the rs880890 enhancer significantly reduces CALCRL levels, especially under disturbed flow conditions.
- Highlighted essential function of CALCRL in endothelial cells, mediating key signaling pathways (eNOS [endothelial NO synthase], APLN [apelin], angiopoietin, prostaglandins, and endothelin-1) crucial for cell proliferation, tube formation, and NO production.
- Our findings uncover a novel mechanism by which genetic variants and shear stress collaboratively dictate CALCRL expression, offering new insights into the genetic regulation of coronary artery disease risk.

Coronary artery disease (CAD) is a disease of coronary vessels that develops due to the buildup of atherosclerotic plaques in the vessel wall. Genome-wide association studies have identified ≈300 risk loci for CAD, which are beginning to shed light on the complexity of its genetic architecture.[1–5] Although some associations are located within coding regions, ≈98% of signals come from noncoding regions, which suggests that single-nucleotide polymorphisms (SNPs) within gene regulatory elements play a major role in mediating the effects on gene expression.[6–8]

One of the identified CAD genome-wide association study loci on chromosome 2q32.1 harbors the *CALCRL* (calcitonin receptor-like) gene,[1] encoding for a 7-transmembrane G-protein–coupled receptor that mediates the pleiotropic effects of CGRP (calcitonin gene-related peptide) and ADM (adrenomedullin).[9] These 2 structurally related neuropeptides were originally described as potent vasodilators. Beyond blood pressure regulation, CALCRL is involved in a variety of key biological processes, including cell proliferation, modulation of apoptosis, vascular biology, and inflammation, and is currently emerging as a novel target for the therapy of migraine.[10] In solid tumors, antibody-mediated inhibition of CALCRL signaling has been demonstrated to reduce tumor growth via disruption of angiogenesis or via direct antiproliferative effects on cancer cells.[11] Interestingly, it was further shown that CALCRL is expressed in normal CD34+ hematopoietic progenitors, and CGRP and ADM directly act on CD34+ cells to promote colony formation in vitro, indicating a functional role of CALCRL in physiological myelopoiesis[12]

Recently, *CALCRL* was demonstrated to be a major enhancer of the NO pathway in endothelial cells through unidirectional shear stress response.[13] A fundamental function of the endothelial layer of blood vessels is their ability to sense fluid shear stress and transform this information into intracellular signals.[14] These mechanosensing and mechanosignaling processes are critical for maintaining vascular integrity, thus affecting not only physiological vascular tone and morphogenesis but also pathological vascular processes including hypertension and atherosclerosis. In the present study, we demonstrate that the noncoding regulatory region in the 3′ end of *CALCRL* is important for gene expression and show that rs880890, a variant associated with both hypertension and CAD risk, exhibits allele-specific regulatory activity. We further demonstrate that stress regulates this region through the binding of HSF (heat shock factor) transcription factors and silencing of HSF1 significantly reduces CALCRL expression. Overall, our study suggests a causal role for rs880890-carrying enhancer in regulating angiogenesis, proliferation, and NO production where CALCRL plays a key mediator role.

MATERIALS AND METHODS

Data Availability

The RNA-seq experiments reported in this study are deposited in the GEO database under the accession number: GSE222118.

Cells

TeloHAEC (ATCC; CRL-4052), HepG2 (ATCC; HB-8065), RAW 264.7 (ATCC; TIB-71), preadipocyte 3T3-L1 (ATCC; CL-173), and MOVAS (ATCC; CRL-2797) cell lines were used in the luciferase experiment. TeloHAECs were cultured using vascular cell basal medium (ATCC; PCS-100-030) supplemented with Endothelial Cell Growth Kit-vascular endothelial growth factor (ATCC; PCS-100-041) and 10% fetal bovine serum (FBS). HepG2 cells were cultured in DMEM (4.5-g/L glucose, 2-mmol/L L-glutamine; Lonza) supplemented with 10% FBS (GIBCO; Thermo Fisher Scientific). RAW 264.7 was cultured using DMEM and FBS (heat inactivated in the water bath at 56° for 30 minutes). 3T3-L1 was cultured using DMEM (Lonza BE12-614F) supplemented with 10% FBS and 2-mM L-glutamine. MOVAS was cultured using DMEM supplemented with geneticin. Primary human coronary artery endothelial cells were cultured in media MV2 (purchased from Promocell) and used between passages 4 and 6. 100-U/mL penicillin and 100-µg/mL streptomycin were used in all cell lines used in this study to prevent bacterial contamination.

Gene and Enhancer RNA Expression Quantification

Gene transcript coordinates were identified from GRO-seq data using a custom de novo detection pipeline.[15,16] Enhancer RNA (eRNA) quantification was performed using Homer[17] analyzeRepeats.pl, with parameters -noadj, -noCondensing, and -pc 3. Quantification was done from the opposite strand of coding gene transcription for intragenic enhancers and from both strands for intergenic enhancers. Gene end coordinates were expanded by 1500 bp to account for transcription at the end of transcripts and annotating intragenic gene enhancers. Counts for eRNA and gene expression were normalized using the voom[18] function of limma R package. Only enhancers with counts per million >1 in at least 5 samples were included in the analysis.

Elastic Net Regression

The elastic net multivariable regression model was applied to individual genes using eRNA as predictive variables. This approach was aimed at identifying the enhancers that are most effective in predicting gene expression. For each gene, only enhancers that were in the same topologically associating domain and $P<0.05$ from the Spearman correlation test of significance were used for fitting the model. Caret[19] and glmnet[20] R packages and the repeatedcv method with 5 repeats and folds set to 5 were used for tuning and cross-validating the model. This process involved running the model across a range of α values from 0 to 1 in increments of 0.05 and recording the mean cross-validated error at the lambda.min value. Here, α and λ are regularization parameters. α controls the balance between the L1 (Lasso) and L2 (ridge) regularization terms. A higher α emphasizes fewer coefficients, while a lower α leans toward ridge regularization. Enhancers for a given gene were ranked based on their model coefficient to determine their importance for predicting gene expression. Model coefficients refer to the weights assigned to each feature in the predictive model. Therefore, when the model was fitted to predict gene expression values using enhancer expression values, the best enhancers got higher coefficients and were ranked higher than enhancers with coefficients close to zero.

Clustered Regularly Interspaced Short Palindromic Repeats/Clustered Regularly Interspaced Short Palindromic Repeat–Associated 9–Mediated Enhancer Deletion

The CRISPR reagents were adapted from the Alt-R system from IDT. The guide RNAs were designed using the IDT tool to minimize off-targeting effects using 2 guides to create 372-bp deletion (Table S1). The positive control (crRNA targeting HPRT) from the Alt-R clustered regularly interspaced short palindromic repeats/clustered regularly interspaced short palindromic repeat–associated 9 Human Control Kit (IDT) was used. Delivery of the ribonucleoprotein complex into TeloHAEC was performed using a Neon Transfection System with a 1350-V pulse of 30 ms width. Forty-eight hours after transfection, RNA was purified using an RNeasy Mini Kit (Qiagen) and the cDNA was prepared with a RevertAid First Strand cDNA Synthesis Kit (Thermo Fisher Scientific). The mRNA level of the CALCRL was measured by SYBR green chemistry quantitative polymerase chain reaction (PCR) using specific primers (Table S2) in a StepOne Real-Time PCR System (Thermo Fisher Scientific). Three independent experiments with 4 technical replicates were performed. Data (ΔCt values) were checked for normal distribution using the Shapiro-Wilk test and the F test to compare variance before performing statistical tests, and the unpaired *t* test (2-tailed) was used. $P<0.05$ was used to define a significant difference between the groups. To generate clones (ΔEnh) with an enhancer deletion, cells underwent electroporation and were dispensed into a 96-well plate using a single-cell dilution technique. These cells were subsequently cultivated until clones exhibited the desired enhancer deletion.

Single-Cell RNA-seq Data Processing and Analysis

scRNA-seq data previously generated from atherosclerotic human coronary arteries[21] were obtained from the NCBI GEO repository (accession number GSE131778). The data processing and cell type annotation were performed as described in the study by Örd et al[22] using the Seurat package.[23] For plotting gene expression in individual cells, the gene counts were depth-normalized to 10 000 total counts per cell and log-transformed.

Dual-Luciferase Reporter Assays

DNA fragments containing the region rs880890-rs840585 with haplotypes G-T and A-C were amplified by PCR from genomic DNA with Phusion polymerase and specific primers (Table S3). For the dual-luciferase reporter assay, amplified DNA (698 bp) was subcloned into the hSTARR-seq_ORI plasmid (Addgene, No. 99296) that was used as a backbone for the plasmid constructs. The enhancer-inserted plasmid was cotransfected into TeloHAEC, HepG2, RAW 264.7, preadipocyte 3T3-L1, and MOVAS cell lines with the control vector pGL4.75 (Promega), which encodes the luciferase gene *hRluc* (*Renilla reniformis*). The luciferase constructs prepared with the inserts were verified by sequencing. Luciferase plasmids with minimal promoter containing rs840588(A)_rs840587(C), rs840588(G)_rs840587(A),

rs907463(T), and rs907463(G) enhancers were purchased from vector builder. Transfection was performed in a 6-well plate using Lipofectamine Stem Transfection Reagent (Thermo Fisher Scientific; STEM00008) according to the protocol, and the Dual-Luciferase Reporter Assay System (Promega; E1980) was used to detect luciferase activity. Three independent experiments with 4 technical replicates were performed. Data followed a normal distribution (Shapiro-Wilk test) and equal variance (F test). Hence, the unpaired Student *t* test (2-tailed) was used for comparing enhancer activity in regions carrying rs880890 A allele compared with G.

Self-Transcribing Active Regulatory Region Sequencing Allelic Reporter Assay Processing

TeloHAEC and HepG2 cell lines were used for the experiment. Self-transcribing active regulatory region sequencing library and experiment have been described previously by Örd et al,[22] Selvarajan et al,[24] and Toropainen et al.[25] To assess the transcriptional activity of haplotypes of the candidate regulatory regions, self-transcribing active regulatory region sequencing RNA read data were UMI-deduplicated, depth-normalized to library size, and normalized for haplotype abundance in the plasmid DNA (input) library.

Motif Analysis of rs880890

To identify the potential transcription factors binding to the region with rs880890, PERFECTOS-APE[26] was used with TFBS motif collection, *P* value cutoff of 0.0005, fold change cutoff of 2.0, and motifbreakR[27] package with default settings.

Endothelial Cell Chromatin Immunoprecipitation Assay-seq/ATAC-seq Data Analysis Related to Athero-Relevant Flows

Because TeloHAECs are homozygous to the region of the SNP rs880890, the following chromatin immunoprecipitation assay (ChIP)-seq data related to endothelial cells (HUVEC) cultured under shear stress (for 6 hours at 37 °C and with constant CO_2 perfusion at ±3 dyn/cm^2) and static were downloaded from GSE116241. Sequencing data were downloaded from NCBI using the SRA toolkit and processed using the nf-core ChIP-seq pipeline[28] to derive BAM files. The BaalChIP[29] tool was used for allele-specific measurements of transcription factor binding from the ChIP-seq data. A Bayesian statistical approach was used by the tool to correct the effect of background allele frequency on the observed ChIP-seq read counts. ATAC-seq data related to human aortic endothelial cells (HAECs) that were heterozygous at rs880890 undergoing shear stress were downloaded from GSE112340. Reads were aligned to hg19 with Bowtie2.[30] SAMtools[31] was used to convert sam to BAM files. BAM files were sorted and indexed using the SAMtools sort and index function. IGV viewer[32] was used to visualize the SNP position and count the read counts in unidirectional flow (UF) and disturbed flow (DF).

HSF1 Knockdown and CALCRL Expression Under Athero-Relevant Flows

A flow device consisting of a computerized stepper motor UMD-17 (Arcus Technology) and a 1° tapered stainless steel cone was used to generate the physiologically relevant shear stress pattern.[33] The flow device was placed in a 37 °C incubator with 5% CO_2. The flow patterns used for this experiment can be found in Table S4. HAECs were seeded in 6-well plates at 100% confluence and cultured in flow media with EGM-2 medium (Lonza) containing 4% dextran. HAECs were subjected to UF or DF for 24 hours[33] before being harvested for RNA isolation. HAECs were seeded in 6-well plates in EGM-2 medium at 90% confluence and were transfected with 50-nmol/L siRNA using RNAiMAX (Life Technologies) as described by the manufacturer. siRNA targeting HSF1 (SI03246348) and nontargeting controls (1027310) were both purchased from Qiagen. Media was changed the following day to flow media with EGM-2 medium containing 4% dextran. HAECs were subjected to UF for another 24 hours[33] before being harvested for RNA isolation. RNA was isolated from cells using GenElute Mammalian Total RNA Miniprep Kit (Sigma-Aldrich) and reverse transcribed using a High-Capacity cDNA Reverse Transcription Kit (Thermo Fisher). Quantitative mRNA expression was determined by reverse transcriptase-quantitative PCR using SYBR Green MasterMix (Roche, Indianapolis, IN). The mRNA level of the HSF1 knockdown under shear stress was measured by using specific primers (Table S5).

Dual-Luciferase Reporter Assays Under Athero-Relevant Flows

For the luciferase reporter assay, the following flow setup was used. Ibidi Pump System Quad (10906; ibidi GmbH) and Ibidi µ-Slide VI with ibiTreat surface and channel height of 0.4 mm, length of 17 mm, and width of 3.8 mm (80606; ibidi GmbH) were used. Channels were first coated with PureCol collagen solution (5005; Advanced BioMatrix). Next, TeloHAECs (0.8×10^5) were seeded into the channel in the vascular cell basal medium. After cell attachment, channels were rinsed once with medium, and perfusion sets (red, 10962; ibidi GmbH) were installed in the pump system. A shear stress of 10 dyn/cm^2 was first established for 30 minutes to allow the cells to adapt for flow, followed by an increase in shear stress to 20 dyn/cm^2 for 45 to 46 hours. For DF, an oscillatory flow setup for the Ibidi Pump System was used with 20 dyn/cm^2 and a switching time of 2 s (ie, 0.25 Hz). The flow rate remains constant except during valve switching simulating oscillatory turbulence.[34] The fluid velocity using the µ-Slide VI 0.4 10 dynes was 7.89 mL/min and 20 dynes was 15.77 mL/min. The viscosity (0.0072 dyns/cm^2) of the fluid is a typical value for a cell culture medium supplemented with FBS at 37 °C. The formula used to calculate shear stress is given as follows: $\tau=\eta 176.1\Phi$ where Φ is the flow rate (mL/min), τ is the shear stress (dyn/m^2), and η is the dynamical viscosity (dyns/cm^2). For luciferase assay, channels were first rinsed twice with PBS, dry trypsinized, and channels were rinsed with lysis buffer to collect the cells. Data followed a normal distribution (Shapiro-Wilk test) and equal variance (F test). Hence, the unpaired Student *t* test (2-tailed) was used for comparing enhancer activity between rs880890_A and rs880890_G.

siRNA-Mediated Knockdown of CALCRL

For the siRNA treatment, TeloHAECs were reverse transfected with the Lipofectamine RNAiMAX transfection reagent

(Thermo Fisher) according to the manufacturer's instructions. The target-specific Silencer Select siRNAs for *CALCRL* (s19889 and s19890) and scrambled siRNA were obtained from Thermo Fisher. Cells were lysed 24 hours after transfection. Three independent experiments with 4 technical replicates were performed. RNA extraction, cDNA synthesis, quantitative PCR, and statistical analysis followed the protocol described above for clustered regularly interspaced short palindromic repeats/clustered regularly interspaced short palindromic repeat–associated 9 experiments. The knockdown efficiency was >95%.

ChIP-Quantitative PCR Under Athero-Relevant Flows

For the ChIP-quantitative PCR, the flow setup was the same as used in HSF1 Knockdown and CALCRL Expression Under Athero-Relevant Flows section. The flow device was placed in a 37 °C incubator with 5% CO_2. TeloHAECs at 100% confluence, maintained in EGM-2 medium containing 4% dextran (Sigma-Aldrich) in 6-well plates, were subjected to athero-protective UF or athero-susceptible DF for 24 hours before cells were processed for ChIP analysis. TeloHAECs subjected to UF or DF for 24 hours were cross-linked, digested, and immunoprecipitated according to the manual instruction of Pierce Agarose ChIP Kit (Thermo Scientific). Briefly, cells subjected to flow were washed with warm PBS before cross-linking with 1% formaldehyde. After a 10-minute incubation, glycine was added to 125-mmol/L final concentration, and, after 5 minutes, the cells were pelleted down and the supernatant was removed. Cells were then resuspended in 1-mL ice-cold PBS and 10-µL protease inhibitors (Halt Cocktail; Pierce) and were pelleted at 3000*g* for 5 minutes before lysing for undergoing MNase digestion at 10 U/µL for 15 minutes. After recovery of digested chromatin, the solution was immunoprecipitated with an anti-HSF1 antibody (Cell Signaling Technology; No. 4356) at 1.1 µg/2×10^6 cells and with normal rabbit IgG as control overnight. After binding to agarose beads, the immunoprecipitate was eluted before DNA cleanup, and then, purified DNA was detected by quantitative PCR performed on LightCycler 480 II (Roche) using SYBR Green I Master (Roche) with primers (Table S6). Statistical analyses were performed with the 2-tailed unpaired Student *t* test.

TeloHAEC Protein Extraction

TeloHAECs were collected (5×10^6) in PBS by scraping from culture flasks and washed twice with cold PBS. Resuspension of cells was done into 500-µL 1× Hypotonic Buffer (20-mmol/L Tris-HCl, pH 7.4, 10-mmol/L NaCl, and 3-mmol/L $MgCl_2$) with protease inhibitor cocktail by pipetting up and down several times, followed by incubation on ice for 15 minutes. Twenty-five microliter of detergent (10% NP40) was added and vortexed for 10 s at the highest setting. Centrifugation was performed of the homogenate for 10 minutes at 3000 rpm at 4 °C. Cytoplasmic fraction in the supernatant was removed. The nuclear pellet was resuspended in 50-µL complete cell extraction buffer (10-mmol/L Tris, pH 7.4, 2-mmol/L Na_3VO_4, 100-mmol/L NaCl, 1% triton X-100, 1-mmol/L EDTA, 10% glycerol, 1-mmol/L EGTA, 0.1% SDS, 1-mmol/L NaF, 0.5% deoxycholate, and 20-mmol/L $Na_4P_2O_7$) for 30 minutes on ice by vortexing at 10-minute intervals followed by sonication, followed by centrifugation for 30 minutes at 14.000*g* at 4 °C. Quantitation of protein concentration was performed using the Quant-iT Protein Quantitation Kit (Thermo Fisher Scientific).

Electromobility Shift Assay

Oligonucleotide probes (Table S7; 15-bp flanking SNP site for reference or alternate allele) with a biotin tag at the 5′ end of the sequence (Integrated DNA Technologies) were incubated with TeloHAEC nuclear extract and the working reagent from the LightShift Chemiluminescent Electromobility Shift Assay Kit (Thermo Fisher Scientific, catalog number: 20148, Rockford, IL). For competitor assays, an unlabeled probe of the same sequence was added to the reaction mixture at 100× excess. The reaction was incubated for 30 minutes at room temperature and then loaded on a 6% retardation gel (Invitrogen, catalog number: EC6365BOX, California). The contents of the gel were transferred to a nylon membrane and visualized by the UV transillumination Image Lab Software (Bio-Rad Laboratories).

Allele-Specific ChIP-Quantitative PCR

HAEC donors (n=2; Major Resources Table) heterozygous for the SNP rs880890 were selected to study the allele-specific binding of the variant to transcription factor HSF1. For ChIP, the experimental setup was the same as used in ChIP-Quantitative PCR Under the Athero-Relevant Flows section. Quantitative PCR was conducted using a custom TaqMan SNP Genotyping Assay for rs880890 (Thermo Fisher). This assay uses allele-specific probes coupled to different fluorescent dyes in the same reaction mix for the quantitative detection of the alleles in a single sample. The rs880890 assay amplifies a 130-bp region around this SNP. We calculated haplotype-specific enrichment for both anti-HSF1 and IgG. Fold enrichment was determined by dividing the enrichment of the immunoprecipitated chromatin by the enrichment of the respective input. The experiment was performed with 3 biological replicates, and quantitative PCR was performed in triplicate. Statistical analyses were performed with the 2-tailed unpaired Student *t* test.

Western Blot for si-CALCRL and Enhancer-Deleted Samples

Five micrometer of total cytoplasmic protein were combined with gel loading buffer, heated to 95 °C for 5 minutes and separated on Any kD Mini-PROTEAN TGX Stain-Free Protein Gels (No. 4568123; Bio-Rad Laboratories). Treated groups were loaded next to their corresponding controls at each time point in each gel. The proteins from enhancer-deleted clone (ΔEnh) and si-CALCRL were transferred to 0.2-µm nitrocellulose membranes (No. 1704158; Bio-Rad Laboratories) using the Trans-Blot Turbo Transfer System (Bio-Rad Laboratories), blocked in 5% nonfat dry milk in TBS-Tween and incubated for 1.5 hours at room temperature and with the primary antibody Anti-CALCRL (1:500, No. PA5-50644; Thermo Fisher Scientific) overnight. After washing, the membranes were incubated with horseradish peroxidase–conjugated anti-rabbit or anti-mouse secondary antibodies (1:2000, No. Sc-2357; Santa Cruz Biotechnology, or 1:1000, No. 7076; Cell Signaling Technology, respectively). The signal was visualized using Pierce ECL Plus Western Blotting Substrate (No. 32134; Thermo

Fisher Scientific) and ChemiDoc (Bio-Rad Laboratories) for imaging. The membranes were stripped after probing with CALCRL primary antibody using RESTORE Western blot stripping buffer (No. PIER21059; Thermo Fisher Scientific) for 45 minutes at 37 °C. The membrane was then reprobed using the GAPDH (1:5000, No. 39-8600; Thermo Fisher Scientific) primary antibody. Three biological replicates were performed. The ratio of CALCRL to GAPDH was calculated using imageJ[35] for each lane, and the values of these ratios were normalized to the control group.

RNA-Sequencing and Data Analysis

For the *CALCRL*-silenced and enhancer-deleted samples, total RNA quality was assessed using the Agilent 2100 Bioanalyzer System. RNA library preparation was handled using QuantSeq 3′ mRNA-seq Library Prep Kit FWD (Lexogen according to the manufacturer's instructions). The library was quantified using Qubit dsDNA HS Assay Kit (Q32854; Thermo Fisher Scientific), and its quality was checked with a Bioanalyzer using High Sensitivity DNA Kit (5067-4626; Agilent Technologies). Individual libraries were pooled in equimolar ratio (4 nmol/L for each) and sequenced on an Illumina NextSeq 500. The bcl2fastq2 v2.20 (Illumina) was used to demultiplex sequencing data and convert base call files into FASTQ files. Nf-core[28] RNA-seq pipeline was used to process FASTQ files and derive gene counts. Gene counts were normalized for effective library size, and differentially expressed genes were analyzed using DESeq2.[36] Differentially expressed genes were defined by $P<0.05$ and an absolute fold change of >2.

Expression of Downstream Target Genes Under Athero-Relevant Flows

Human coronary artery endothelial cells (purchased from Promocell) were seeded on 0.1% gelatin-coated slides with a density of 2.5×10^5 and cultured for a minimum of 3 days to ensure complete confluence, production, and reorganization of subcellular matrix and maturation of cell-cell junctions. Culture underflow was performed for 72 hours using a parallel plate flow apparatus as described[37–39] under DF (5 dyn/cm^2) or UF (1.5 dyn/cm^2) shear stress. Total RNA was extracted from human coronary artery endothelial cells using the RNeasy Mini Kit (Norgen) according to the manufacturer's protocol. 100-ng RNA was reverse transcribed into cDNA with random primer by reverse transcriptase (Qiagen). cDNA (relative 1.7-ng RNA) was amplified by standard quantitative PCR with Taq DNA polymerase (Sensifast, SybrGreen, LOW-ROX Kit; Bioline). The geometric mean of GAPDH, RPLP0, and PABC4 quantification was used to normalize the expression of each test gene. The paired Student *t* test was used for data that followed normal distribution using the Shapiro-Wilk test. $P<0.05$ was used to define a significant difference between the groups (n=7 individual donors).

Network Analysis and Identification of CALCRL Coexpressed Genes

The weighted gene correlation network analysis[40] was used for the identification of coexpressed genes from RNA-seq samples. Weighted gene correlation network analysis is a well-established tool for studying biological networks based on pairwise correlation between variables in high-dimensional RNA-seq data sets. ComBat-seq[41] was used to remove the batch effect from the data. Sequencing data were processed as mentioned in the Data Analysis section. After rlog transformation, we identified the genes, and samples with excessive numbers of missing samples were identified using the function goodSamplesGenesMS and were discarded from the analysis. The samples were then clustered using the function hclust to identify outliers in the data set. We constructed a weighted gene network using soft-thresholding power β. The function pickSoftThreshold was used, which aids in choosing a proper soft-thresholding power. We chose a power of 10, which resulted in an approximate scale-free topology network with the scale-free fitting index R2 >0.9. For the remaining genes, the choice of the soft-thresholding power β was used to which coexpression similarity is raised to calculate adjacency with function adjacency. The matrix of correlations was converted to an adjacency matrix of connection strengths. To minimize the effects of noise and spurious associations, the adjacency was transformed into a topological overlap matrix using TOM, and the corresponding dissimilarity was calculated. The function hclust was used to hierarchically cluster the genes. Branches of the dendrogram group together densely interconnected are highly coexpressed genes. Modules were then defined as sets of genes with high topological overlap. The module hub gene was defined as the gene in the module with the highest connectivity or based on high intramodular connectivity. Cytoscape[42] app geneMANIA[43] was used to identify known and novel coexpressed genes.

To identify how much of the coexpressed genes are enriched in the differential expressed data set of *CALCRL* depletion, a gene enrichment analysis was performed using the hypergeometric *t* test.[44] The parameters for the hypergeometric *t* test are given as follows. The number of successes (k=49) was the coexpressed genes significantly differentially expressed under *CALCRL* depletion ($P<0.05$), the sample size (s=195) was the total coexpressed genes, and the number of successes in the population (M=1460) represented all the genes that were significantly differently expressed under *CALCRL* depletion ($P<0.05$; in both siRNA and enhancer deletion), while population size (N=11 820) was the total number of genes included in the analysis.

Griess and LDH Cytotoxicity Assays

Nitrate Colorimetric Assay Kit (Cayman Chemical; 780001) was used to measure the total nitrate production in an enhancer-deleted clone (ΔEnh). Cells from ΔEnh and control cells (from a similar passage as the enhancer-deleted clones) were plated in Ibidi μ-Slide VI and underwent unidirectional, disturbed, and static conditions as mentioned in Dual-Luciferase Reporter Assays Under Athero-Relevant Flows section. Culture media was collected after 48 hours. Total nitrate/nitrite concentrations of ΔEnh clone and control samples under UF and DF were normalized to static conditions. The assay was performed according to the manufacturer's protocol. The LDH Cytotoxicity Assay Kit (Cayman Chemical; 601170) was used to measure cell death in the treatment of ox-LDL (oxidized low-density lipoprotein; Thermo Fisher; L34357) and LDL (Thermo Fisher; L3486). ΔEnh and control cells were plated in a 96-well plate and subjected to 200-μg/mL ox-LDL and LDL treatment for

24 hours. The assay was performed according to the manufacturer's protocol. Statistical analyses were performed with the unpaired Student *t* test (2-tailed).

Cell Proliferation Assay

Transfected cells were seeded at 5×10^3 cells per well in 200 µL of complete media in E-plates (ACEA Biosciences, San Diego, CA) and grown for 48 hours while monitoring with xCELLigence DP system (ACEA Biosciences) that measures electrical impedance across interdigitated gold microelectrodes integrated on the bottom of tissue culture plates. The xCELLigence recorded cell index readings every 1 hour for 3 days. Three biological replicates were used to determine cell proliferation and represented the relative numbers of cells compared with control cells. A 2-way repeated measures ANOVA test with the Sidak multiple comparisons test was used to compare *CALCRL* siRNA knockout treatment to scrambled (negative) control and ΔEnh clone to control, with $P_{adj}\leq0.05$ deemed significant.

Tube Formation Assay

Forty-eight–well plate was coated with Matrigel basement membrane matrix 150 µL/well (Corning, growth factor reduced). For CALCRL knockdown and ΔEnh clones, TeloHAECs (40 000 cells) were seeded onto the Matrigel 48 hours after siRNA transfection. Knockdown efficiencies of >95% were consistently attained and detected by quantitative PCR. Images were taken from 9 spots per replicate every 4 hours until 24 hours using Incucyte (S3 System). Each siRNA knockdown had 3 technical replicates in each experiment, and experiments were repeated 3×. Analysis was done with ImageJ[35] and associated macro tool Angiogenesis Analyzer[45] where the total tube length was selected as the parameter of evaluation. For time-course analysis, each time point represents the average tube length from all spots of all replicates with the same treatments at the same time point. Data were checked for normal distribution before performing statistical tests. The unpaired Student *t* test (2-tailed) was used for data because values followed a normal distribution and equal variance.

RESULTS

Identification of *CALCRL* Regulatory Enhancer by Coexpression Analysis

CALCRL is a G-protein–coupled receptor and a recently identified CAD locus.[11] Further analysis of the SNPs within the *CALCRL* locus using the Open Target Genetics portal[46] demonstrated that the SNPs are also associated with hypertension (Figure 1A). Because the majority of the variants were located within noncoding regions and overlapped enhancer elements marked by DNase hypersensitivity and H3K27ac, we next sought to identify the relative importance of individual enhancers in the regulation of *CALCRL* expression. Starting from the premise that eRNAs are coexpressed with their target genes,[48,49] we constructed coexpression networks based on regularized logistic regression. This was achieved by comparing coactivity patterns of eRNAs and coding gene expression across cell types based on public GRO-seq data on 336 samples representing 45 cell types.[15] Our model reports a linear combination of coefficients derived from eRNA expression to describe how important each enhancer is as a predictor for gene expression. Complex heatmap[47] of 12 regulatory regions (Figure 1B and 1C) was included in our analysis, and enhancer-8 demonstrated the highest regression coefficient of 0.31 and was, thus, predicted to be central for the regulation of *CALCRL* expression (Table S8). The plot of GRO-seq enhancer-8 eRNA and CALCRL mRNA expression showed a positive correlation with a *P* value of 1.38×10^{-11} (Figure S1A). Hi-C data from TeloHAECs[50] further confirmed the interaction between enhancer-8 and the promoter of *CALCRL* (Figure S1B). Finally, to confirm the predicted regulatory role of enhancer-8 in controlling endothelial *CALCRL* expression, the Alt-R clustered regularly interspaced short palindromic repeats/clustered regularly interspaced short palindromic repeat–associated 9 system was used to selectively delete a 372-bp genomic region in TeloHAECs using electroporation. PCR assays and Western blot detected around 50% genetic deletion in the regulatory region enclosing rs880890 and a reduction in CALCRL expression in TeloHAECs (Figure S2). The enhancer-deleted cells (ΔEnh) exhibited significantly lower gene expression ($P=0.003$) compared with control cells confirming the importance of the enhancer elements in regulating *CALCRL* expression (Figure 1D).

Allele-Specific Activity of rs880890-Harbored Enhancer in TeloHAECs

The enhancer-8 harbored 5 CAD-associated SNPs, and we next focused on characterizing rs880890 and rs840585 in the DNAse hypersensitivity region in more detail. (Figure 1B, zoom out). The GTEX[51] database suggested that *CALCRL* expression is ubiquitous throughout tissues (Figure S3) with the highest expression seen in the lung, the artery, and the adipose tissue. To identify the cell type contributing to the expression of *CALCRL* in the arterial tissue, we took advantage of single-cell data from mouse single-cell atlas (Tabula Muris[52]). tSNE visualization of all tissues from Tabula Muris identified *CALCRL* expression predominantly in endothelial cells (Figure 2A). In addition, analysis of public scRNA-seq data from human atherosclerotic lesions[21] demonstrated high expression of *CALCRL* in endothelial cells and, to a lesser degree, in smooth muscle cells (Figure 2B; Figure S4). In line with the cell type–specific gene expression, enhancer-8 was only found accessible in endothelial cells of the human atherosclerotic aorta based on our previously published single-nucleus ATAC-seq data[22] (Figure 2C).

To study whether the cell type specificity could be driven by enhancer-8, we measured the enhancer

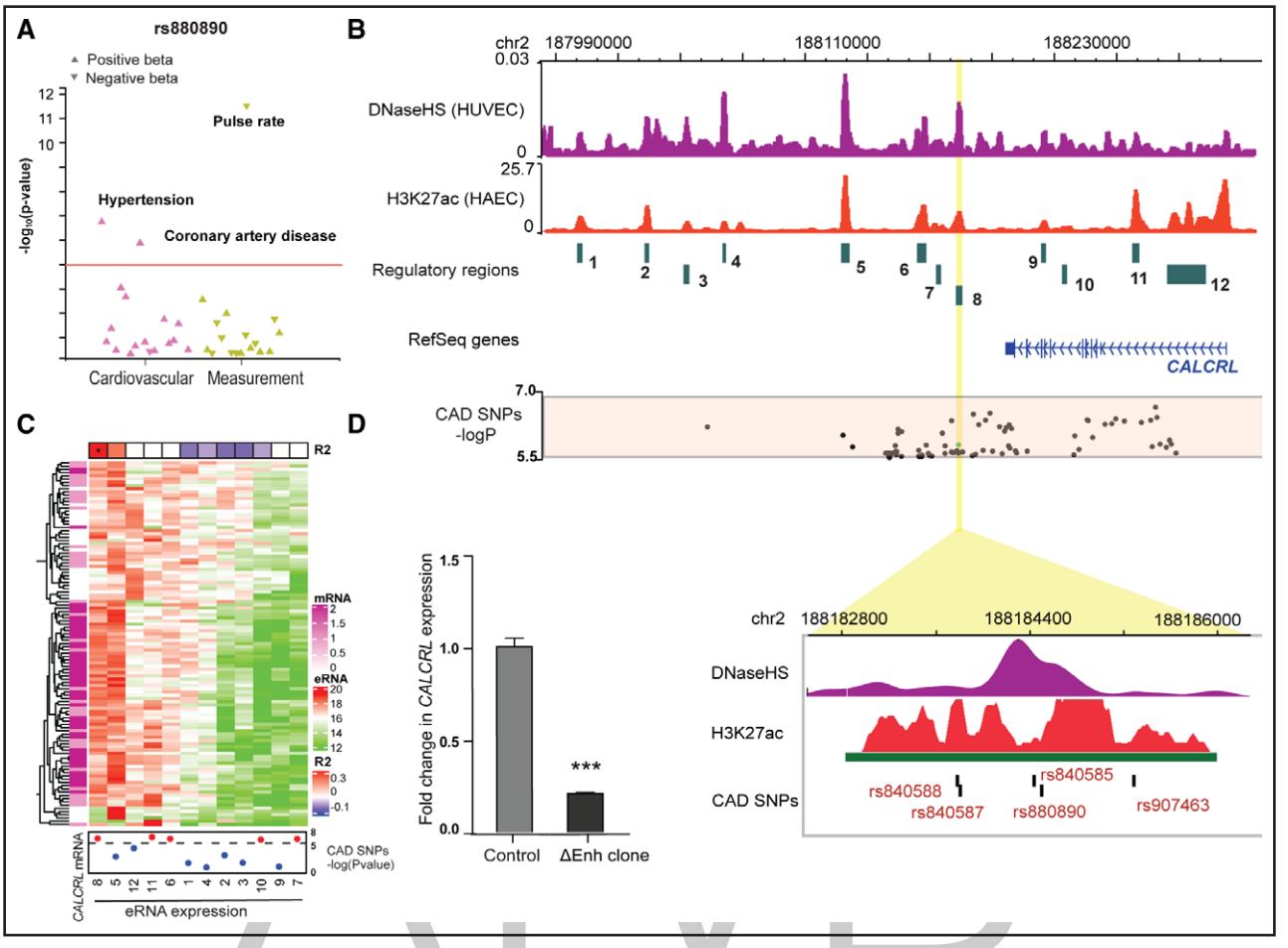

Figure 1. XXX.

A, Association of rs880890 with CVD-related traits from the Open Targets Genetics portal.[46] rs880890 was significantly associated with hypertension and coronary artery disease (CAD). **B**, WashU browser shot of CAD loci with CALCRL (calcitonin receptor-like) region showing the regulatory regions (1–12) included in the study. A close-up look of the enhancer-8 harboring CAD-associated single-nucleotide polymorphisms (SNPs). DNAse hypersensitivity shows that the region with rs880890/rs840585 is accessible compared with nearby regions. **C**, Complex heatmap[47] showing the enhancer RNA expression of each enhancer included in the study, CALCRL mRNA expression, R2 value of enhancers, and the CAD SNPs annotations. **D**, Results of clustered regularly interspaced short palindromic repeats/clustered regularly interspaced short palindromic repeat–associated 9–mediated regulatory region deletion in TeloHAECs (ΔEnh clone). Quantitative polymerase chain reaction was performed in 3 independent experiments. The statistical significance was evaluated using a 2-tailed Student *t* test (unpaired). For the bar plot, significance is denoted with an asterisk. ***P=0.003.

activity of 698-bp region in endothelial cells (TeloHAEC), preadipocytes (3T3L1), smooth muscle cells (MOVAS), hepatocytes (HepG2), and macrophages (RAW 264.7). Enhancer-8 harbored 5 CAD SNPs of which 2 were in the DNase hypersensitive region. The SNPs were assessed through a luciferase assay. While rs840588, rs840587, and rs907463 did not show any difference in enhancer activity (Figure S5A), haplotype (ref: rs880890[A]_rs840585[C] and alt: rs880890[G]_rs840585[T]) showed significant difference compared with the empty plasmid. Low enhancer activity was detected in all cell types except TeloHAECs, which demonstrated 100-fold higher activity. Importantly, when we compared the luciferase signal of the A allele with the G allele, there was a 40% increase in the activity of A compared with G (Figure 2D). This cis-eQTL was confirmed in the GTEx database where the rs880890 A allele was significantly associated with increased expression of CALCRL compared with the G allele (Figure S5B). Also supporting our results, a trend of allele-specific deposition of histone mark H3K27ac and the binding of endothelial-specific transcription factor *ERG* was also detected in a cohort of 21 to 44 HAEC donors[53] (Figure S6A). This is in line with the predicted *ERG* motifs in enhancer-8 situated 238 bp upstream and 291 bp downstream around the HSF1 motif at rs880890 SNP.

To separate between the 2 SNPs in mediating the allele-specific effect, we cloned the naturally occurring 3 haplotype combinations into a reporter vector with haplotype 1 containing the reference alleles rs880890(A) and rs840585(C) while haplotype 2 carrying rs880890(G) allele and haplotype 3 rs840585(T) allele. Our analysis

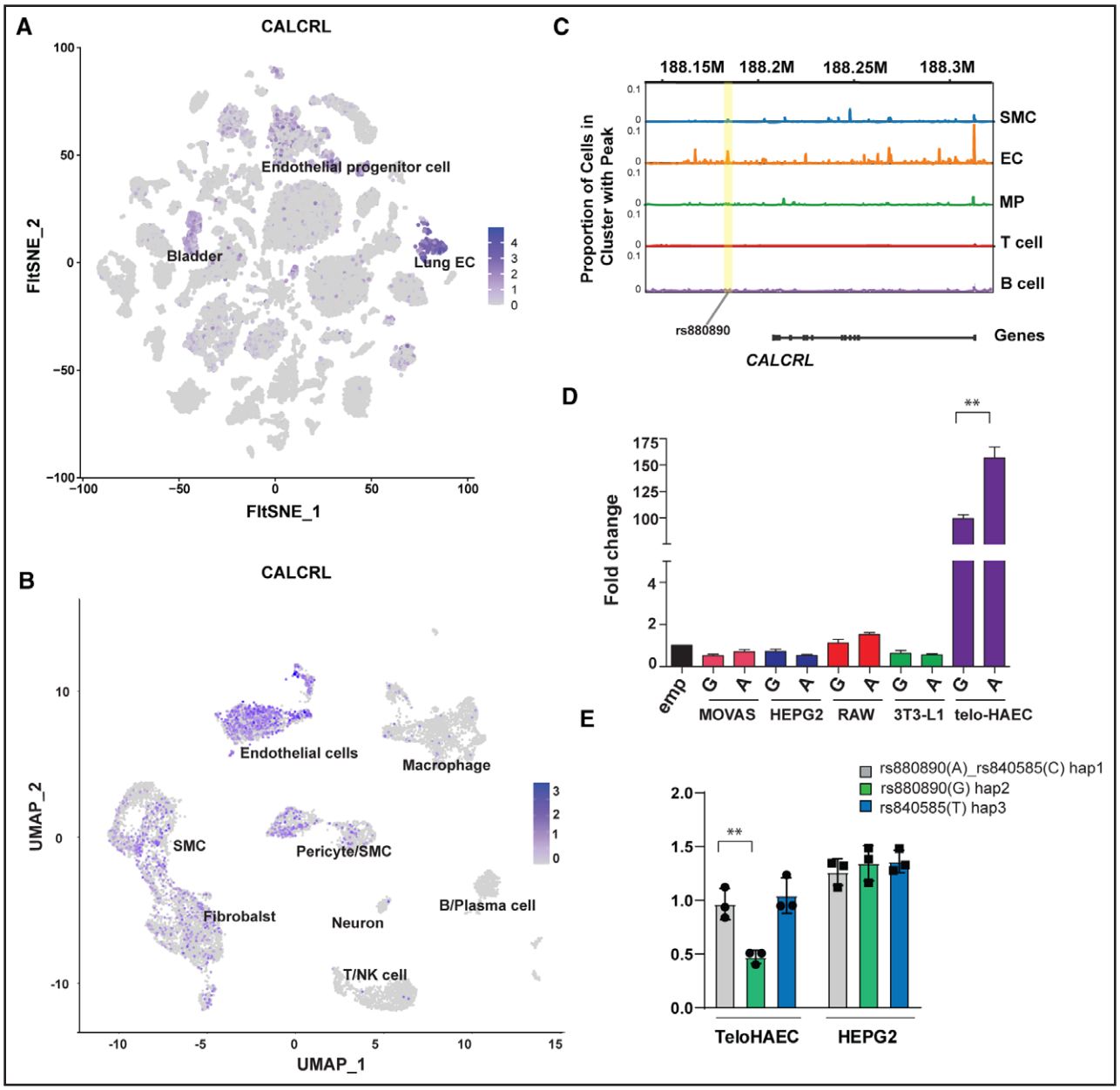

Figure 2. XXX.

A, Single-cell RNA-seq data from Tabula Muris[52] representing data across 20 organs and tissues from mice show that CALCRL (calcitonin receptor-like) is highly expressed in endothelial cells, especially in the lung. **B**, Single-cell RNA-seq data from human coronary arteries[21] demonstrating that CALCRL is predominantly expressed in endothelial cells followed by smooth muscle cells and fibroblasts. **C**, Pseudobulk coverage track visualization of single-nucleus ATAC-seq signal[22] at the CALCRL loci showing endothelial cell type–specific activity of the rs880890-containing regulatory element. **D**, The activity of the rs880890-containing enhancer was investigated in MOVAS, HEPG2, RAW 264.7, 3T3-L1, and TeloHAECs. Luciferase assay shows a significant increase in enhancer activity in regions carrying the rs880890 A allele compared with the G allele in TeloHAEC followed by RAW 264.7, while other cell types did not show enhancer activity. **E**, Self-transcribing active regulatory region sequencing results from TeloHAEC and HepG2 showing the enhancer activity in the presence of rs880890 or rs840585. Results show that a difference in enhancer activity was observed only in the presence of rs880890 in TeloHAEC, and no difference in enhancer activity in HepG2 was seen (n=3). The statistical significance was evaluated using a 2-tailed Student *t* test (unpaired). For the bar plot, significance is denoted with an asterisk. ***P*<0.01.

suggests that compared with haplotype 1, only haplotype 2 showed allele-specific enhancer activity, while hap3 showed no effect (Figure 2E), pinpointing rs880890 as the most probable causal SNP. Importantly, rs880890 also demonstrated significant evolutionary conservation (PhyloP −log *P*=0.57) compared with rs840585 that was predicted to be fast evolving (PhyloP −log *P*=−0.99).[54] To understand the allele-specific binding of transcription factors to the rs880890, we performed an electromobility shift assay using biotinylated 31-bp probes targeting

either the reference or alternative allele in TeloHAECs. Competitor assays were performed by incubating the reaction with ×100 excess of unlabeled (no biotin) oligonucleotide complexes with identical sequences (Figure S7). The results demonstrated an increased protein binding to the A allele compared with the G allele of rs880890 (Figure 3A). The sequence-based motif analysis revealed that HSFs such as HSF1, HSF2, and HSF4 are likely to bind to the *CALCRL*-regulating enhancer at the rs880890 SNP region with a preference toward the A allele in binding affinity (Figure S8; Table S9). HSFs are known to activate heat shock proteins during stress,[55] and in endothelial cells, HSF1 increase corresponds to elevated levels of eNOS (endothelial NO synthase).[56] To further explore this, allele-specific ChIP-quantitative PCR was conducted to assess HSF1 binding in heterozygous HAEC donors, using a custom TaqMan Genotyping Assay for rs880890. Confirming motif predictions, HSF1 showed a 1.63-fold higher enrichment at the A allele compared with the G allele (donor 1: P=0.004; donor 2: P=0.007; Figure 3B).

Cis-Regulatory Element, rs880890, and CALCRL Are All Flow Responsive

As CALCRL is a key enhancer of the eNOS pathway implicated in fluid shear stress response and HSF1[57] has been shown to be activated by shear stress, we wanted to investigate the effect of rs880890 SNP on enhancer activity under such conditions. As expected, ECs exhibited morphological changes under UF, DF, and static flow conditions (Figure S9). Luciferase assay confirmed significantly lower enhancer activity after HSF1 knockdown, while an even further decrease in the luciferase activity of enhancers was observed under DF compared with UF (Figure 3C and 3D). ATAC-seq analysis of HAECs subjected to UF mimicking hemodynamics in the human distal carotid artery or the DF waveform mimicking the hemodynamics in the human carotid demonstrated that the rs880890-harboring enhancer is more accessible in HAECs under UF compared with DF (Figure 3E). Moreover, analysis of the publicly available H3K27ac ChIP-seq data allowed us to interrogate the allelic bias of rs880890 under shear stress in endothelial cells. The results confirmed that the A allele is indeed biased toward higher enhancer activity binding compared with the G allele, and this effect is more prominent under shear stress in HAECs and HUVECs (Figure 3F; Table S10). These effects were concordant with the regulation of *CALCRL* expression, which was higher in HAECs subjected to UF and lower in DF (P<0.001; Figure 3G). HSF1 knockdown under UF (Figure 3H) resulted in a significant decrease in *CALCRL* expression. This is in line with the directionality of HSF1 expression under shear stress with lower HSF1 levels detected under DF compared with UF.[58] In contrast, *ERG* knockout resulted in no significant change in CALCRL expression under UF, whereas we did note a significant decrease under DF. This suggests a potential coregulatory relationship between *ERG* and HSF1 (Figure S6B). To further validate the anticipated binding of HSF1 to enhancer-8, we conducted a targeted HSF1 ChIP-PCR. Our findings revealed a marked reduction in HSF1 binding to the enhancer region in HAECs under DF conditions compared with UF (Figure 3I), thus confirming that shear stress alters the binding of HSF1 to the enhancer.

CALCRL Knockdown and Enhancer-Deleted Cells Affect Vasodilation and Endothelial-Specific Pathways

To understand the downstream effects of *CALCRL* and *CALCRL*-regulating enhancers, we performed RNA-seq on siRNA-mediated *CALCRL* knockdown and CRISPR-mediated rs880890-enhancer deletion. We then used the rlog-transformed matrix of our RNA-seq data to construct a coexpression network using 11 820 genes across 22 samples. This allowed the identification of 31 distinct gene coexpression modules in our RNA-seq data depicted in distinct colors (Figure S10). The *CALCRL* gene was found in the module blue along with 143 coexpressed genes. A dendrogram of consensus module eigengenes obtained on the consensus correlation was used to merge the similar modules blue and cyan with a threshold of 0.1 resulting in the identification of 195 genes coexpressed with *CALCRL*. Selected genes are illustrated on a geneMANIA network (Figure 4A) that demonstrates the relationships between CALCRL and coexpressed genes. Interestingly, we observed potentially new *CALCRL* coexpressed genes, such as *APLN* (apelin), *ADAMTS18*, and *AKAP12*.

Further analysis of the differentially expressed genes identified 390 and 990 genes significantly regulated (P_{adj}<0.05) upon gene silencing or enhancer deletion, respectively (Tables S11 and S12). Importantly, this included 25% of the 195 *CALCRL* coexpressed genes, demonstrating significant enrichment (hypergeometric *t* test P=6.5×10^{-7}). Functional enrichment analysis demonstrated that similar pathways were regulated by both the gene and enhancer repression (Figure 4B). The most important pathways affected included the repression of APLN, EDN1 (endothelin-1), ADM, eNOS, and angiopoietin signaling pathways. *APLN* and cyclooxygenase (*PTGS2*) genes themselves were significantly downregulated in both RNA-seq experiments, indicating they could be direct downstream targets of CALCRL (Figure 4C and 4D). Among the differentially expressed genes, *PTGS1* and *PTGS2* were also downregulated in DF compared with UF further linking these genes to shear stress (Figure S11A and S11B). Interestingly, we also observed a downregulation trend of *EDN1*. The RNA-seq results also indicated that depletion of

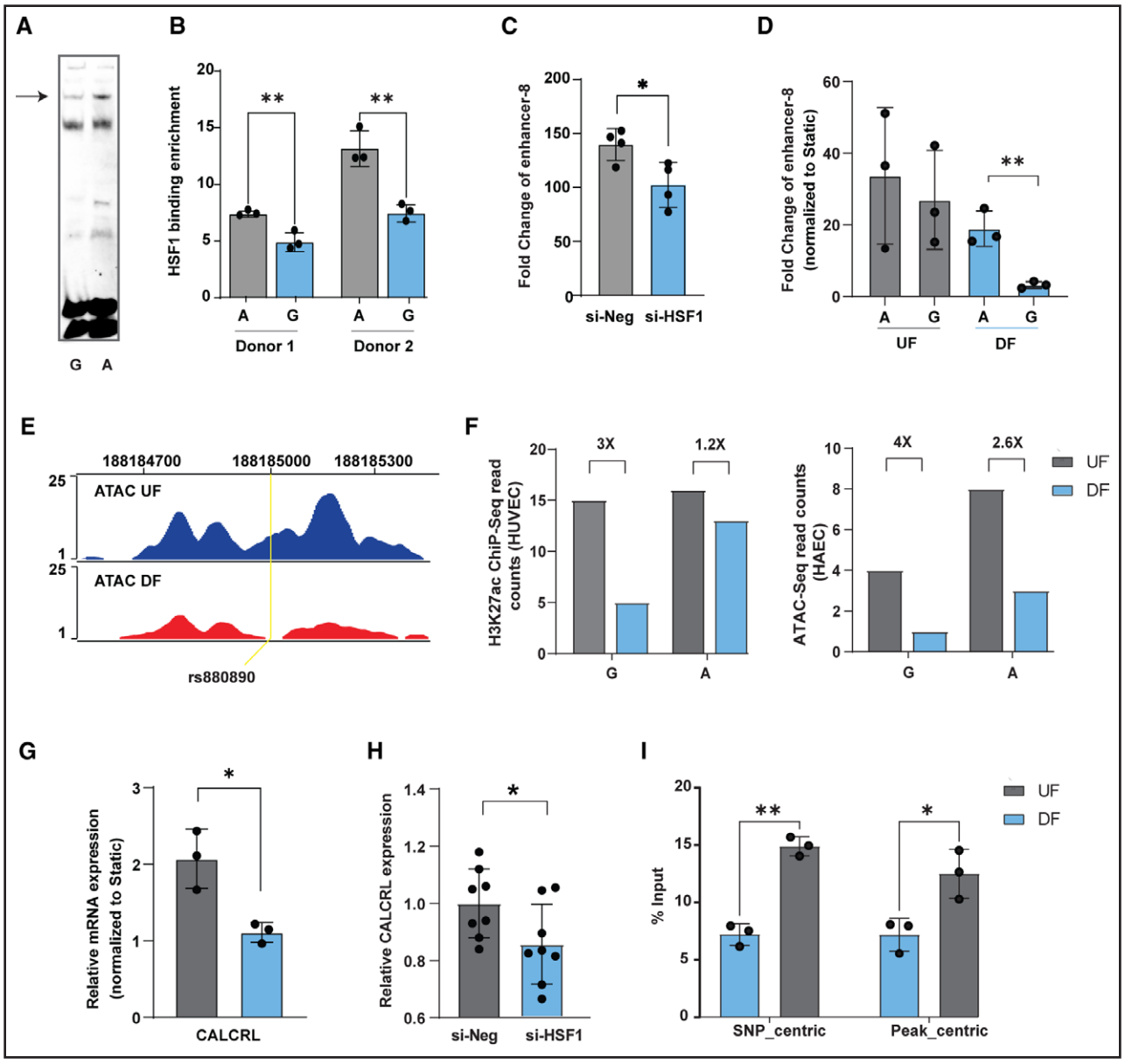

Figure 3. XXX.

A, Electromobility shift assay for the rs880890 single-nucleotide polymorphism (SNP) showing (arrow pointing) that the A allele significantly gains binding affinity with the G allele. **B**, Allele-specific chromatin immunoprecipitation assay (ChIP)-quantitative polymerase chain reaction (PCR) showing 1.63-fold higher enrichment of HSF1 (heat shock factor 1) binding at A allele compared with G allele (donor 1: P=0.004; donor 2: P=0.007). **C**, Luciferase assay showing a significant decrease in enhancer-8 activity during HSF1 knockdown. **D**, Luciferase assay showing a further decrease in enhancer-8 activity under disturbed flow (DF) compared with unidirectional flow (UF) in the presence of G allele. **E**, ATAC-seq demonstrating higher accessibility of the rs880890 cis-regulatory element (enhancer-8) in human aortic endothelial cells (HAECs) under UF compared with DF. **F**, Increased ATAC-seq and ChIP-seq reads in rs880890-containing region in HAECs under UF compared with DF. The bar plot shows increased ATAC/ChIP-seq reads in cells under UF and lower reads from the G allele–containing chromosome under DF compared with the A allele. **G**, A significant decrease (P<0.01) in the expression of CALCRL (calcitonin receptor-like) was detected under DF compared with UF. **H**, Knockdown of HSF1 under shear stress resulted in significant downregulation of CALCRL expression (P=0.02). **I**, HSF1 ChIP-PCR showed significant changes in binding activity in HAEC under DF when compared with UF. The condition was true for both SNP-centric (binding detection with rs880890 at the center) and peak-centric (enhancer-8 peak's center). The statistical significance of the experiments in the figure was evaluated using a 2-tailed Student t test (unpaired). For the bar plot, significance is denoted with an asterisk. *P<0.05 and **P<0.01. si-Neg indicates siNegative.

CALCRL expression leads to repression of TGF-β signaling (*THBS1*, *PTGS2*, and *TGFBR2*) and angiogenesis regulatory genes (*PDPK1* and *ANGPTL4*). In line with this, knockdown of *CALCRL* and enhancer deletion led to a significant decrease in cell proliferation (Figure 5A and 5B) and tube formation (Figure 5C–5E).

Finally, we performed an LDH cytotoxicity assay on ΔEnh clones to assess the effect of LDL (200 μg/mL)

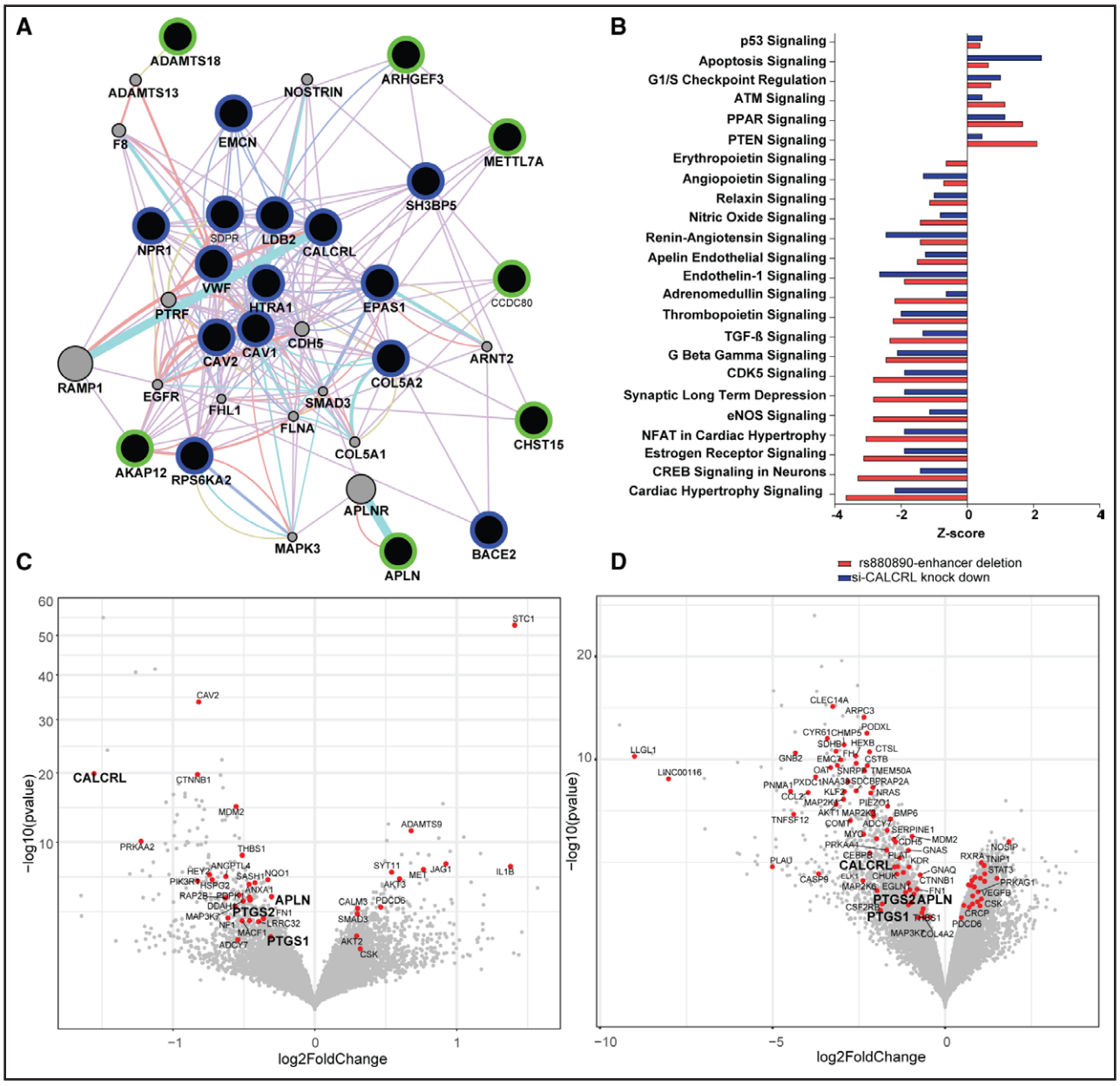

Figure 4. XXX.

A, Network generated by Cytoscape app geneMANIA. Black nodes with blue outlines represent known CALCRL (calcitonin receptor-like) coexpressed genes, while black nodes with green borders are novel coexpressed genes. Purple connection denotes coexpression, cyan denotes pathway, pink denotes physical interaction, and purple denotes colocalization. **B**, Functional enrichment plot of CALCRL siRNA and rs880890 enhancer–deleted samples using IPA. *Z* score indicates a predicted activation or inhibition of a pathway (ie, erythropoietin, angiopoietin, relaxin, NO, renin-angiotensin, apelin endothelial, endothelin-1, adrenomedullin, thrombopoietin, and eNOS (endothelial NO synthase) signaling pathways are predicted to be repressed). **C** and **D**, Volcano plot highlighting selected candidates differentially expressed in RNA-seq data from CALCRL siRNA and rs880890 enhancer–deleted samples.

and ox-LDL (200 µg/mL) on cell viability. The results demonstrated that the ox-LDL treatment induces a significant increase (P=0.026) in cell growth in the ΔEnh clone (Figure 5F) compared with control cells. To explore the difference in the production of NO underflow, ΔEnh clones and control cells were exposed to UF and DF followed by detection of NO production by using the Griess assay. In our results, as shown in Figure 5G and Figure S11C, we observe that ΔEnh clones under DF showed a significant reduction in NO production compared with UF (P=0.035) further confirming the vital role of enhancer-8 in the regulation of CALCRL for NO production.

DISCUSSION

Blood flows through the arteries with the tangential frictional force that acts on the surface of endothelial cells.[59] The frictional force, or shear stress, spans a range of

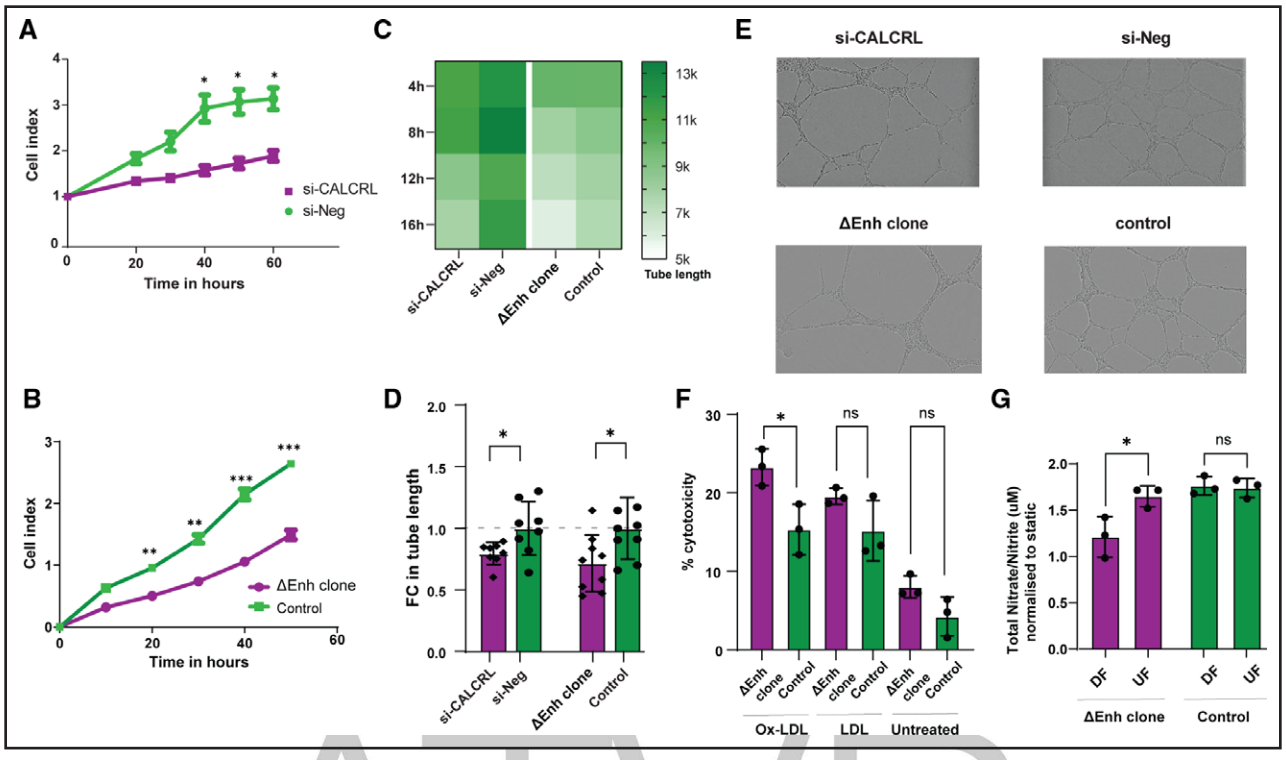

Figure 5. XXX.

A and **B**, Effect of CALCRL (calcitonin receptor-like) downregulation on proliferation of TeloHAECs. Normalized cell index (xCELLigence system) on siRNA knockdown of CALCRL (si-CALCRL) and enhancer-deleted clone (ΔEnh clone) in TeloHAECs shows a significant decrease in cell proliferation. A 2-way repeated measures ANOVA test with the Sidak multiple comparison tests for CALCRL siRNA treatment vs scrambled negative controls and ΔEnh clone vs control at each time point: **P*<0.05, ***P*<0.01m and ****P*<0.001. Data points are average values of 3 biological replicates. **C**, Effect of si-CALCRL and ΔEnh clone on tube formation. Heat map of the averaged total tube lengths 4 to 16 hours after plating TeloHAECs on Matrigel (n=3). **D**, Fold change (FC) in tube length formation. Each bar represents the average+SEM of total tube lengths obtained from each well image. Tube length values comparing si-CALCRL to siNegative (si-Neg; *P*=0.026) and ΔEnh clone (*P*=0.023) to control were used and analyzed by 2-tailed Student *t* test. **P*<0.05. **E**, Representative of 9-spot well output images from Incucyte after 24 hours of si-CALCRL treatment (n=3) and ΔEnh clones (n=3). **F**, ox-LDL (oxidized low-density lipoprotein; 200 µg/mL) and LDL (200 µg/mL) induced cell death in enhancer-deleted clone (ΔEnh clone) and control cells (TeloHAEC with similar passage as ΔEnh clone). ox-LDL–induced cytotoxicity showed significantly higher cytotoxicity in ΔEnh clones (*P*=0.026). **G**, NO production in ΔEnh clone and control cells (TeloHAEC with similar passage as ΔEnh clone). NO production was detected by Griess assay (n=3); total nitrate/nitrite concentration was significantly downregulated in disturbed flow (DF) compared with unidirectional flow (UF; *P*=0.035) in clones. For the bar plots, the statistical significance was evaluated using a 2-tailed Student *t* test (unpaired). Significance is denoted with an asterisk. **P*<0.05.

spatiotemporal scales and contributes to regional and focal heterogeneity of endothelial gene expression, which is important in vascular pathology.[60] To this end, exposure to multidirectional disturbed blood flow at arterial bifurcations and curves primes endothelial activation, promoting pathological processes that contribute to atherosclerosis, the major cause of CAD.[61] UF/shear stress promotes eNOS expression and activity, lack of which contributes to the development of atherosclerosis at DF sites. Krause et al[62] recently reported that the noncoding common variant at rs17114036, associated with CAD/IS in a genome-wide association study, regulates *PLPP3* expression in the endothelium through increased enhancer activity that is dynamically regulated by UF and transcription factor KLF2. Here, we extend the discovery and characterization of genetic variants associated with CAD acting through shear stress regulation by identifying a mechanosensitive endothelial enhancer that regulates *CALCRL* expression. Specifically, we identified a noncoding, common genetic variant rs880890 that modified levels of *CALCRL* expression in endothelial cells. We demonstrate that rs880890 confers increased enhancer activity that is dynamically regulated by UF and HSF transcription factors.

Our data suggest that decreased endothelial production of CALCRL could be associated with atherosclerosis. Endothelial-specific deficiency of CALCRL has previously been shown to lead to increased formation of atherosclerotic lesions in mice.[59] In addition to CAD, the 2q32.1 locus is also associated with hypertension. In line with this, in our study, the G allele at rs880890 is associated with an increased risk for hypertension.[63] Because the G allele of rs880890 reduces the CALCRL production, which is normally needed to increase cAMP levels and activate PKA (protein kinase A) and eNOS,[13] reduced NO production could explain its association with hypertension.

Interestingly, the minor allele frequency (G) of rs880890 is highly variable between the ethnicities ranging from 0.2 in the African population to 0.9 in Asian populations such as Japanese,[64] suggesting population-specific differences in the risk susceptibility mediated by this locus.

Vasoreactivity is an important characteristic of blood vessels to maintain adequate supply to perfused tissues dependent on required metabolic needs. eNOS-derived NO is an endogenous vasodilatory gas that continually regulates the diameter of blood vessels and maintains an antiproliferative and antiapoptotic environment in the vessel wall.[65] Our data from perturbation experiments demonstrate that CALCRL could play a major role in the regulation of several vasodilatory factors. To this end, we identify APLN[66] and EDN1[67,68] as potential downstream targets of CALCRL. Although we did not observe a difference in NO production in DF compared with UF flow and in nonflow static conditions, the difference in NO production was observed in the ΔEnh clone under DF compared with UF. In addition, PTGS1 (COX-1) and PTGS2 (COX-2), key enzymes that convert arachidonic acid to prostaglandins to mediate vasodilation and inhibition of platelet aggregation,[69] were identified. Further investigations are warranted to shed light on the involvement of CALCRL in regulating the expression of *APLN*, *PTGS1*, *PTGS2*, and *EDN1*.

CALCRL/ADM/G-protein-α activation in endothelial cells has been shown as a promising approach to inhibit the progression of atherosclerosis by reducing endothelial inflammation.[59] In this study, we provide in vitro evidence that *CALCRL* expression is regulated by the concerted action of genetic variation and shear stress to promote pathogenic mechanisms leading to plaque formation. We present a model where the G allele of rs880890 associated with increased risk of CAD confers decreased endothelial enhancer activity, thereby reducing *CALCRL* expression. Under DF, changes in histone acetylation limit DNA accessibility, further reducing HSF1/2/4 binding and *CALCRL* expression. Changes in *CALCRL* expression may influence vasoconstriction and atherosclerotic plaque formation through the regulation of eNOS, APLN, ADM, renin-angiotensin, angiopoietin, and EDN1 signaling pathways with reduced expression promoting pathology. In summary, this study has identified a previously unreported mechanosensitive pathway and HSFs as important transcription factors that exert an antiatherosclerotic effect in endothelial cells. Our data highlight the utility of using genome-wide association study data to illuminate the molecular mechanisms that drive pathology and provide a plausible mechanism for how human SNPs in *CALCRL* regulate cardiovascular disease.

ARTICLE INFORMATION

Received January 5, 2023; accepted March 25, 2024.

Affiliations

A.I. Virtanen Institute for Molecular Sciences (I.S., M.K., T.Ö., K.Õ., M.G., A.R., K.M., A.T., J.P.L., M.K.-M.) and Institute of Biomedicine, School of Medicine (P.P., M.H.), University of Eastern Finland, Kuopio. Department of Cellular and Molecular Medicine, College of Medicine, The University of Arizona, Tucson (A.K.G., L.K.S., C.E.R.). Department of Medicine, The University of Chicago, IL (R.-T.H., J.L., J.Z., Y.F.). Department of Immunology, Genetics and Pathology, Uppsala University, Sweden (M.A., P.U.M.). Faculty of Medical Sciences, Biosciences Institute, Newcastle University, United Kingdom (S.W.).

Acknowledgments

The authors wish to acknowledge Biocenter Finland for infrastructure support and the CSC – IT Center for Science, Finland, and the Bioinformatics Center of the University of Eastern Finland for the computational resources. The graphic abstract was created with BioRender.com.

Sources of Funding

This research was supported by the European Research Council under the European Union's Horizon 2020 Research and Innovation Program (grant 802825 to M. Kaikkonen-Määttä), the Academy of Finland (grants 287478 and 319324 to M. Kaikkonen-Määttä and grants 321535 and 353376 to J.P. Laakkonen), the National Institutes of Health (NIH; grants R01HL147187/HL/NHLBI NIH HHS/United States to C.E. Romanoski), the American Heart Association (grant 20PRE35200195 to L.K. Stolze), the Swedish Research Council (grants 2013-9279 and 2021-01919 to P.U. Magnusson), the Academy of Finland (grants 276634 and 312487 to P. Pölönen and M. Heinäniemi), the Instrumentarium Science Foundation (to I. Selvarajan), the Finnish Cultural Foundation (to I. Selvarajan), the Finnish Foundation for Cardiovascular Research (to I. Selvarajan and J.P. Laakkonen), the Sigrid Jusélius Foundation (to M. Kaikkonen-Määttä), and the Doctoral Program of Molecular Medicine at the University of Eastern Finland.

Disclosures

None.

Supplemental Material

Figures S1–S11
Tables S1–S12
Major Resources Table

REFERENCES

1. van der Harst P, Verweij N. Identification of 64 novel genetic loci provides an expanded view on the genetic architecture of coronary artery disease. *Circ Res.* 2018;122:433–443. doi: 10.1161/CIRCRESAHA.117.312086
2. Nikpay M, Goel A, Won HH, Hall LM, Willenborg C, Kanoni S, Saleheen D, Kyriakou T, Nelson CP, Hopewell JC, et al. A comprehensive 1000 genomes-based genome-wide association meta-analysis of coronary artery disease. *Nat Genet.* 2015;47:1121–1130. doi: 10.1038/ng.3396
3. Koyama S, Ito K, Terao C, Akiyama M, Horikoshi M, Momozawa Y, Matsunaga H, Ieki H, Ozaki K, Onouchi Y, et al. Population-specific and trans-ancestry genome-wide analyses identify distinct and shared genetic risk loci for coronary artery disease. *Nat Genet.* 2020;52:1169–1177. doi: 10.1038/s41588-020-0705-3
4. Assimes T, Tcheandjieu C, Zhu X. A large-scale multi-ethnic genome-wide association study of coronary artery disease [published online March 10, 2021]. doi: 10.21203/RS.3.RS-275591/V1
5. Aragam KG, Jiang T, Goel A, Kanoni S, Wolford BN, Atri DS, Weeks EM, Wang M, Hindy G, Zhou W, et al; Biobank Japan. Discovery and systematic characterization of risk variants and genes for coronary artery disease in over a million participants. *Nat Genet.* 2022;54:1803–1815. doi: 10.1038/s41588-022-01233-6
6. Engel KL, Mackiewicz M, Hardigan AA, Myers RM, Savic D. Decoding transcriptional enhancers: evolving from annotation to functional interpretation. *Semin Cell Dev Biol.* 2016;57:40–50. doi: 10.1016/j.semcdb.2016.05.014
7. Gloss BS, Dinger ME. Realizing the significance of noncoding functionality in clinical genomics. *Exp Mol Med.* 2018;50:1–8. doi: 10.1038/s12276-018-0087-0
8. Brnne I, Civelek M, Vilne B, Di Narzo A, Johnson AD, Zhao Y, Reiz B, Codoni V, Webb TR, Foroughi Asl H, et al; Leducq Consortium CAD Genomics. Prediction of causal candidate genes in coronary artery disease loci. *Arterioscler Thromb Vasc Biol.* 2015;35:2207–2217. doi: 10.1161/ATVBAHA.115.306108
9. Angenendt L, Bormann E, Pabst C, Alla V, Görlich D, Braun L, Dohlich K, Schwöppe C, Bohlander SK, Arteaga MF, et al. The neuropeptide

receptor calcitonin receptor-like (CALCRL) is a potential therapeutic target in acute myeloid leukemia. *Leukemia*. 2019;33:2830–2841. doi: 10.1038/s41375-019-0505-x
10. Russell FA, King R, Smillie SJ, Kodji X, Brain SD. Calcitonin gene-related peptide: physiology and pathophysiology. *Physiol Rev*. 2014;94:1099–1142. doi: 10.1152/physrev.00034.2013
11. Toda M, Suzuki T, Hosono K, Hayashi I, Hashiba S, Onuma Y, Amano H, Kurihara Y, Kurihara H, Okamoto H, et al. Neuronal system-dependent facilitation of tumor angiogenesis and tumor growth by calcitonin gene-related peptide. *Proc Natl Acad Sci USA*. 2008;105:13550–13555. doi: 10.1073/pnas.0800767105
12. Harzenetter MD, Keller U, Beer S, Riedl C, Peschel C, Holzmann B. Regulation and function of the CGRP receptor complex in human granulopoiesis. *Exp Hematol*. 2002;30:306–312. doi: 10.1016/s0301-472x(02)00772-5
13. Iring A, Jin YJ, Albarrán-Juárez J, Siragusa M, Wang SP, Dancs PT, Nakayama A, Tonack S, Chen M, Künne C, et al. Shear stress-induced endothelial adrenomedullin signaling regulates vascular tone and blood pressure. *J Clin Invest*. 2019;129:2775–2791. doi: 10.1172/JCI123825
14. Roux E, Bougaran P, Dufourcq P, Couffinhal T. Fluid shear stress sensing by the endothelial layer. *Front Physiol*. 2020;11:861. doi: 10.3389/fphys.2020.00861
15. Bouvy-Liivrand M, Hernández de Sande A, Pölönen P, Mehtonen J, Vuorenmaa T, Niskanen H, Sinkkonen L, Kaikkonen MU, Heinäniemi M. Analysis of primary microRNA loci from nascent transcriptomes reveals regulatory domains governed by chromatin architecture. *Nucleic Acids Res*. 2017;45:9837–9849. doi: 10.1093/nar/gkx680
16. Moreau PR, Bosch VT, Bouvy-Liivrand M, Õunap K, Örd T, Pulkkinen HH, Pölönen P, Heinäniemi M, Ylä-Herttuala S, Laakkonen JP, et al. Profiling of primary and mature miRNA expression in atherosclerosis-associated cell types. *Arterioscler Thromb Vasc Biol*. 2021;41:2149–2167. doi: 10.1161/ATVBAHA.121.315579
17. Heinz S, Benner C, Spann N, Bertolino E, Lin YC, Laslo P, Cheng JX, Murre C, Singh H, Glass CK. Simple combinations of lineage-determining transcription factors prime cis-regulatory elements required for macrophage and B cell identities. *Mol Cell*. 2010;38:576–589. doi: 10.1016/j.molcel.2010.05.004
18. Law CW, Chen Y, Shi W, Smyth GK. voom: precision weights unlock linear model analysis tools for RNA-seq read counts. *Genome Biol*. 2014;15:R29–R17. doi: 10.1186/gb-2014-15-2-r29
19. Kuhn M. Classification and Regression Training [R package caret version 6.0-88]. 2021. Accessed September 8, 2021. https://CRAN.R-project.org/package=caret
20. Friedman J, Hastie T, Tibshirani R. Regularization paths for generalized linear models via coordinate descent. *J Stat Softw*. 2010;33:1–22. Accessed September 8, 2021. https://www.jstatsoft.org/v33/i01/
21. Wirka RC, Wagh D, Paik DT, Pjanic M, Nguyen T, Miller CL, Kundu R, Nagao M, Coller J, Koyano TK, et al. Atheroprotective roles of smooth muscle cell phenotypic modulation and the TCF21 disease gene as revealed by single-cell analysis. *Nat Med*. 2019;25:1280–1289. doi: 10.1038/s41591-019-0512-5
22. Örd T, Õunap K, Stolze L, Aherrahrou R, Nurminen V, Toropainen A, Selvarajan I, Lönnberg T, Aavik E, Ylä-Herttuala S, et al. Single-cell epigenomics and functional fine-mapping of atherosclerosis GWAS loci. *Circ Res*. 2021;129:240–258. doi: 10.1161/CIRCRESAHA.121.318971
23. Hao Y, Hao S, Andersen-Nissen E, Mauck WM, Zheng S, Butler A, Lee MJ, Wilk AJ, Darby C, Zager M, et al. Integrated analysis of multimodal single-cell data. *Cell*. 2021;184:3573–3587.e29. doi: 10.1016/j.cell.2021.04.048
24. Selvarajan I, Toropainen A, Garske KM, López Rodríguez M, Ko A, Miao Z, Kaminska D, Õunap K, Örd T, Ravindran A, et al. Integrative analysis of liver-specific non-coding regulatory SNPs associated with the risk of coronary artery disease. *Am J Hum Genet*. 2021;108:411–430. doi: 10.1016/j.ajhg.2021.02.006
25. Toropainen A, Stolze LK, Örd T, Whalen MB, Torrell PM, Link VM, Kaikkonen MU, Romanoski CE. Functional noncoding SNPs in human endothelial cells fine-map vascular trait associations. *Genome Res*. 2022;32:409–424. doi: 10.1101/gr.276064.121
26. Vorontsov IE, Kulakovskiy IV, Khimulya G, Nikolaeva DD, Makeev VJ. PERFECTOS-APE: predicting regulatory functional effect of SNPs by approximate P-value estimation. BIOINFORMATICS 2015 - 6th International Conference on Bioinformatics Models, Methods and Algorithms, Proceedings; Part of 8th International Joint Conference on Biomedical Engineering Systems and Technologies, BIOSTEC 2015. 2015:102–108.
27. Coetzee SG, Coetzee GA, Hazelett DJ. motifbreakR: an R/Bioconductor package for predicting variant effects at transcription factor binding sites. *Bioinformatics*. 2015;31:3847–3849. doi: 10.1093/bioinformatics/btv470
28. Ewels PA, Peltzer A, Fillinger S, Patel H, Alneberg J, Wilm A, Garcia MU, Di Tommaso P, Nahnsen S. The nf-core framework for community-curated bioinformatics pipelines. *Nat Biotechnol*. 2020;38:276–278. doi: 10.1038/s41587-020-0439-x
29. de Santiago I, Liu W, Yuan K, O'Reilly M, Chilamakuri CSR, Ponder BAJ, Meyer KB, Markowetz F. BaalChIP: Bayesian analysis of allele-specific transcription factor binding in cancer genomes. *Genome Biol*. 2017;18:39. doi: 10.1186/s13059-017-1165-7
30. Langmead B, Salzberg SL. Fast gapped-read alignment with Bowtie 2. *Nat Methods*. 2012;9:357–359. doi: 10.1038/nmeth.1923
31. Li H, Handsaker B, Wysoker A, Fennell T, Ruan J, Homer N, Marth G, Abecasis G, Durbin R; 1000 Genome Project Data Processing Subgroup. The sequence alignment/map format and SAMtools. *Bioinformatics*. 2009;25:2078–2079. doi: 10.1093/bioinformatics/btp352
32. Robinson JT, Thorvaldsdóttir H, Winckler W, Guttman M, Lander ES, Getz G, Mesirov JP. Integrative genomics viewer. *Nat Biotechnol*. 2011;29:24–26. doi: 10.1038/nbt.1754
33. Dai G, Kaazempur-Mofrad MR, Natarajan S, Zhang Y, Vaughn S, Blackman BR, Kamm RD, García-Cardeña G, Gimbrone MA. Distinct endothelial phenotypes evoked by arterial waveforms derived from atherosclerosis-susceptible and -resistant regions of human vasculature. *Proc Natl Acad Sci USA*. 2004;101:14871–14876. doi: 10.1073/pnas.0406073101
34. Sabine A, Bovay E, Demir CS, Kimura W, Jaquet M, Agalarov Y, Zangger N, Scallan JP, Graber W, Gulpinar E, et al. FOXC2 and fluid shear stress stabilize postnatal lymphatic vasculature. *J Clin Invest*. 2015;125:3861–3877. doi: 10.1172/JCI80454
35. Schneider CA, Rasband WS, Eliceiri KW. NIH Image to ImageJ: 25 years of image analysis. *Nat Methods*. 2012;9:671–675. doi: 10.1038/nmeth.2089
36. Love MI, Huber W, Anders S. Moderated estimation of fold change and dispersion for RNA-seq data with DESeq2. *Genome Biol*. 2014;15:550. doi: 10.1186/s13059-014-0550-8
37. Teasdale JE, Hazell GGJ, Peachey AMG, Sala-Newby GB, Hindmarch CCT, McKay TR, Bond M, Newby AC, White SJ. Cigarette smoke extract profoundly suppresses TNFα-mediated proinflammatory gene expression through upregulation of ATF3 in human coronary artery endothelial cells. *Sci Rep*. 2017;7:1–10. doi: 10.1038/srep39945
38. White SJ, Hayes EM, Lehoux S, Jeremy JY, Horrevoets AJG, Newby AC. Characterization of the differential response of endothelial cells exposed to normal and elevated laminar shear stress. *J Cell Physiol*. 2011;226:2841–2848. doi: 10.1002/jcp.22629
39. Hazell GGJ, Peachey AMG, Teasdale JE, Sala-Newby GB, Angelini GD, Newby AC, White SJ. PI16 is a shear stress and inflammation-regulated inhibitor of MMP2. *Sci Rep*. 2016;6:1–11. doi: 10.1038/srep39553
40. Langfelder P, Horvath S. WGCNA: an R package for weighted correlation network analysis. *BMC Bioinf*. 2008;9:1–13. doi: 10.1186/1471-2105-9-559/FIGURES/4
41. Zhang Y, Parmigiani G, Johnson WE. ComBat-seq: batch effect adjustment for RNA-seq count data. *NAR Genom Bioinform*. 2020;2:lqaa078. doi: 10.1093/nargab/lqaa078
42. Shannon P, Markiel A, Ozier O, Baliga NS, Wang JT, Ramage D, Amin N, Schwikowski B, Ideker T. Cytoscape: a software environment for integrated models of biomolecular interaction networks. *Genome Res*. 2003;13:2498–2504. doi: 10.1101/gr.1239303
43. Warde-Farley D, Donaldson SL, Comes O, Zuberi K, Badrawi R, Chao P, Franz M, Grouios C, Kazi F, Lopes CT, et al. The GeneMANIA prediction server: biological network integration for gene prioritization and predicting gene function. *Nucleic Acids Res*. 2010;38:W214–W220. doi: 10.1093/nar/gkq537
44. Hypergeometric t-test. https://systems.crump.ucla.edu/hypergeometric/index.php
45. Carpentier G, Martinelli M, Courty J, Cascone I. Angiogenesis analyzer for ImageJ. 4th ImageJ User & Developer Conference. 2012. Accessed September 7, 2021. https://scholar.google.com/scholar_lookup?hl=en&publication_year=2012&pages=198-201&conference=In%3A+4th+ImageJ+User+%26+Developer+Conference%3B+Mondorf-les-Bains%2C+Luxembourg&author=G+Carpentier&author=M+Martinelli&author=J+Courty&author=I+Cascone&title=Angiogenesis+analyzer+for+ImageJ
46. Ghoussaini M, Mountjoy E, Carmona M, Peat G, Schmidt EM, Hercules A, Fumis L, Miranda A, Carvalho-Silva D, Buniello A, et al. Open Targets Genetics: systematic identification of trait-associated genes using large-scale genetics and functional genomics. *Nucleic Acids Res*. 2021;49:D1311–D1320. doi: 10.1093/nar/gkaa840
47. Gu Z, Eils R, Schlesner M. Complex heatmaps reveal patterns and correlations in multidimensional genomic data. *Bioinformatics*. 2016;32:2847–2849. doi: 10.1093/bioinformatics/btw313

48. Kaikkonen MU, Spann NJ, Heinz S, Romanoski CE, Allison KA, Stender JD, Chun HB, Tough DF, Prinjha RK, Benner C, et al. Remodeling of the enhancer landscape during macrophage activation is coupled to enhancer transcription. *Mol Cell*. 2013;51:310–325. doi: 10.1016/j.molcel.2013.07.010
49. Andersson R, Gebhard C, Miguel-Escalada I, Hoof I, Bornholdt J, Boyd M, Chen Y, Zhao X, Schmidl C, Suzuki T, et al. An atlas of active enhancers across human cell types and tissues. *Nature*. 2014;507:455–461. doi: 10.1038/NATURE12787
50. Lalonde S, Codina-Fauteux VA, de Bellefon SM, Leblanc F, Beaudoin M, Simon MM, Dali R, Kwan T, Lo KS, Pastinen T, et al. Integrative analysis of vascular endothelial cell genomic features identifies AIDA as a coronary artery disease candidate gene. *Genome Biol*. 2019;20:133. doi: 10.1186/s13059-019-1749-5
51. Lonsdale J, Thomas J, Salvatore M, et al. The Genotype-Tissue Expression (GTEx) project. *Nat Genet*. 2013. doi: 10.1038/ng.2653
52. Schaum N, Karkanias J, Neff NF, et al. Single-cell transcriptomics of 20 mouse organs creates a Tabula Muris. *Nature*. 2018;562:367–372. doi: 10.1038/s41586-018-0590-4
53. Stolze LK, Conklin AC, Whalen MB, López Rodríguez M, Õunap K, Selvarajan I, Toropainen A, Örd T, Li J, Eshghi A, et al. Systems genetics in human endothelial cells identifies non-coding variants modifying enhancers, expression, and complex disease traits. *Am J Hum Genet*. 2020;106:748–763. doi: 10.1016/j.ajhg.2020.04.008
54. Nassar LR, Barber GP, Benet-Pagès A, Casper J, Clawson H, Diekhans M, Fischer C, Gonzalez JN, Hinrichs AS, Lee BT, et al. The UCSC Genome Browser database: 2023 update. *Nucleic Acids Res*. 2022;51:13–14. doi: 10.1093/NAR/GKAC1072
55. Zhang Y, Chou SD, Murshid A, Prince TL, Schreiner S, Stevenson MA, Calderwood SK. The role of heat shock factors in stress-induced transcription. *Methods Mol Biol*. 2011;787:21–32. doi: 10.1007/978-1-61779-295-3_2
56. Uchiyama T, Atsuta H, Utsugi T, Oguri M, Hasegawa A, Nakamura T, Nakai A, Nakata M, Maruyama I, Tomura H, et al. HSF1 and constitutively active HSF1 improve vascular endothelial function (heat shock proteins improve vascular endothelial function). *Atherosclerosis*. 2007;190:321–329. doi: 10.1016/j.atherosclerosis.2006.03.037
57. Du J, Li SK, Guan LY, Guo Z, Yin JF, Gao L, Kawanishi T, Shimada A, Zhang QP, Zheng LS, et al. Mechanically sensitive HSF1 is a key regulator of left-right symmetry breaking in zebrafish embryos. *iScience*. 2023;26:107864. doi: 10.1016/j.isci.2023.107864
58. Yeh CF, Cheng SH, Lin YS, Shentu TP, Huang RT, Zhu J, Chen YT, Kumar S, Lin MS, Kao HL, et al. Targeting mechanosensitive endothelial TXNDC5 to stabilize eNOS and reduce atherosclerosis in vivo. *Sci Adv*. 2022;8:eabl8096. doi: 10.1126/SCIADV.ABL8096
59. Nakayama A, Albarrán-Juárez J, Liang G, Roquid KA, Iring A, Tonack S, Chen M, Müller OJ, Weinstein LS, Offermanns S. Disturbed flow–induced Gs-mediated signaling protects against endothelial inflammation and atherosclerosis. *JCI Insight*. 2020;5:e140485. doi: 10.1172/jci.insight.140485
60. Davies PF. Hemodynamic shear stress and the endothelium in cardiovascular pathophysiology. *Nat Clin Pract Cardiovasc Med*. 2009;6:16–26. doi: 10.1038/ncpcardio1397
61. Chiu JJ, Chien S. Effects of disturbed flow on vascular endothelium: pathophysiological basis and clinical perspectives. *Physiol Rev*. 2011;91:327–387. doi: 10.1152/physrev.00047.2009
62. Krause MD, Huang RT, Wu D, Shentu TP, Harrison DL, Whalen MB, Stolze LK, Di Rienzo A, Moskowitz IP, Civelek M, et al. Genetic variant at coronary artery disease and ischemic stroke locus 1p32.2 regulates endothelial responses to hemodynamics. *Proc Natl Acad Sci USA*. 2018;115:E11349–E11358. doi: 10.1073/pnas.1810568115
63. UKBB. http://www.nealelab.is/uk-biobank/
64. dbSNP-database for single nucleotide polymorphisms and other classes of minor genetic variation - PubMed. Accessed January 3, 2023. https://pubmed.ncbi.nlm.nih.gov/10447503/
65. Sessa WC. eNos at a glance. *J Cell Sci*. 2004;117:2427–2429. doi: 10.1242/jcs.01165
66. Helker CSM, Eberlein J, Wilhelm K, Sugino H, Malchow J, Schuermann A, Baumeister S, Kwon HB, Maischein HM, Potente M, et al. Apelin signaling drives vascular endothelial cells towards a pro-angiogenic state. *Elife*. 2020;9:1–44. doi: 10.7554/ELIFE.55589
67. Schneider MP, Boesen EI, Pollock DM. Contrasting actions of endothelin ETA and ETB receptors in cardiovascular disease. *Annu Rev Pharmacol Toxicol*. 2007;47:731–759. doi: 10.1146/annurev.pharmtox.47.120505.105134
68. Davenport AP, Hyndman KA, Dhaun N, Southan C, Kohan DE, Pollock JS, Pollock DM, Webb DJ, Maguire JJ. Endothelin. *Pharmacol Rev*. 2016;68:357–418. doi: 10.1124/pr.115.011833
69. Cannon CP, Cannon PJ. Physiology: COX-2 inhibitors and cardiovascular risk. *Science*. 2012;336:1386–1387. doi: 10.1126/science.1224398